Proceedings of ASME Turbo Expo 2011
GT2011
June 6-10, 2011, Vancouver, British Columbia, Canada

GT2011-46150

INFLUENCE OF MICROJET INJECTION ON SUPERSONIC JET NOISE AND FLOW FIELD

Ryuichi Okada
School of Engineering
University of Tokyo
Tokyo, Japan

Toshinori Watanabe
Department of Aeronautics and Astronautics
University of Tokyo
Tokyo, Japan

Seiji Uzawa
Department of Aeronautics and Astronautics
University of Tokyo
Tokyo, Japan

Takehiro Himeno
Department of Aeronautics and Astronautics
University of Tokyo
Tokyo, Japan

Tsutomu Oishi
IHI Corporation
Tokyo, Japan

ABSTRACT

Jet noise reduction is essential for realization of environmentally-friendly and highly-efficient supersonic jet engines for future civil transport. In the present study, experimental and numerical investigations were conducted to clarify the effect of microjet injection on supersonic jet noise. The experiments were focused on supersonic jet with Mach number up to 1.49 that was generated from a rectangular nozzle with high aspect ratio. Far field acoustic measurements were executed and the spectra and sound pressure data of jet noise were obtained. In order to understand the mechanism of noise reduction, flow field visualization was performed with shadowgraph technique. CFD analysis was conducted as well to observe the flow field and to estimate thrust loss due to the microjet injection.

1. INTRODUCTION

The reduction of noise around airports is one of the urgent and crucial matters for aircrafts and engines. Since supersonic jet generates a significant amount of noise that most people find extremely unpleasant, it is required to reduce the noise dramatically for the realization of supersonic transportation under strict noise regulations. Meanwhile, noise reduction must be accomplished with a minimum loss of the thrust efficiency. Many works have therefore been dedicated to develop various kinds of methods for reducing jet noise. Some of the techniques, mostly passive, are modification of the nozzle exit, use of non-axisymmetric nozzle shapes[1)], and the use of tabs[2)] or chevrons[3)]. Though these techniques have shown substantial noise reduction capability, there are demands for alternative techniques to reduce noise more efficiently. In particular, those which do not interfere with the primary nozzle flow and which can be actively controlled are required.

The use of microjet is one of the promising techniques. Alvi et al.[4)] found that the use of microjets could be very effective in eliminating screech and impingement tones from supersonic jets. Castelain et al.[5)] parametrically studied the effect of microjets on supersonic round jet, focusing on injected mass flux, the number of microjets, the microjets layout and the microjet diameter. Greska et al.[6)] injected several microjets into the supersonic exhaust jet of F404 engine and confirmed reduction of supersonic jet noise. Zaman et al.[7)8)] also parametrically investigated the effects of microjet on acoustic field. They conducted a large matrix of tests against subsonic[7)] and supersonic[8)] main jets, changing the conditions of microjet such as pressure, medium, diameter and number of microjet.

In the previous studies of microjet injection techniques, the nozzle geometries were limited to circular ones. In the present study, on the other hand, a high aspect-ratio rectangular nozzle was adopted as the jet nozzle. It was expected that the combination of non-circular nozzle and microjet injection could be effective for supersonic jet noise reduction based on the literature knowledge[1)] of low-noise characteristics of non-circular nozzles. The nozzle was equipped with forty-four evenly spaced micro-nozzles at the long sides of the nozzle exit.

In our previous studies, effects of microjet injection on supersonic jet noise generated from rectangular jet[9)] and effects on steady flow field[10] had been investigated using acoustic measurement, flow field visualization and CFD analysis under such motivations. However, relationship between acoustic field and flow field was not clarified in these studies. Furthermore, the influence on the thrust has not been investigated. In the present study, therefore, unsteady flow field visualization and thrust estimation by using CFD results have been conducted in addition to the continuation of detailed acoustic and aerodynamic measurements.

2. NOMENCLATURE

M	Mach number of main jet	[-]
P	Total pressure of main jet	[Pa]
P_m	Total pressure of microjet	[Pa]
P_e	Static pressure at nozzle exit	[Pa]
P_a	Ambient air pressure	[Pa]
θ	Elevation angle of measurement point	[deg.]
ϕ	Azimuthal angle of measurement point	[deg.]
ψ	Mass flux ratio of microjet against main jet	[%]
h	Nozzle exit height	[m]
d	Diameter of microjet injection hole	[m]
s	Spacing between active microjet holes	[m]
I	Impulse function	[N]

3. EXPERIMENTAL AND NUMERICAL METHOD

3.1. TEST FACILITY

Experiments were conducted in an anechoic chamber schematically shown in Fig.1. A high-pressure air compressor with maximum storage pressure of 0.83MPa drives the facility. The jet exhausts into the anechoic chamber that measures 5m in width, 7m in length and 3.7m in height. The storage tank provides a total capacity of 60m^3. After leaving the storage tank, the air is separated into two ducts for the main jet and the microjet. The total pressure of the main jet and the microjet can be controlled independently. The mass flux of microjet is measured by mass flow meter and the air for microjet is stagnated at the manifolds. Total pressures of main jet (P) and microjet (P_m) are measured at the settling chamber and the manifolds, respectively.

Figure 2 shows the supersonic jet nozzle with microjet injection holes. A two-dimensional convergent-divergent nozzle was used. The nozzle exit has a rectangular shape with a width of 72mm and a height of 7.7mm. Its throat height is 6 mm. Aspect ratio at the nozzle exit is approximately 9.4. The section from the throat to the exit has a flat surface, and the exit height was slightly changed, if necessary, to adjust the exit Mach number. The rectangular nozzle was adopted to

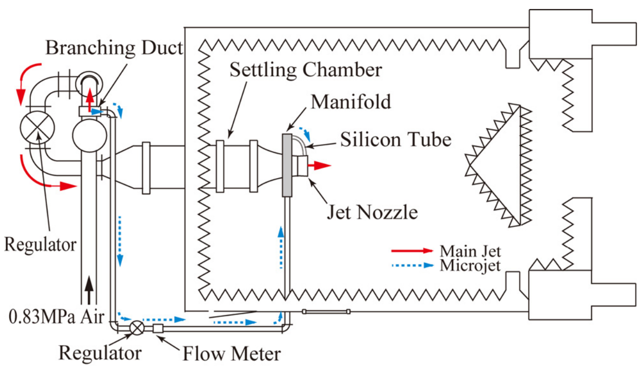

Figure 1 Anechoic chamber

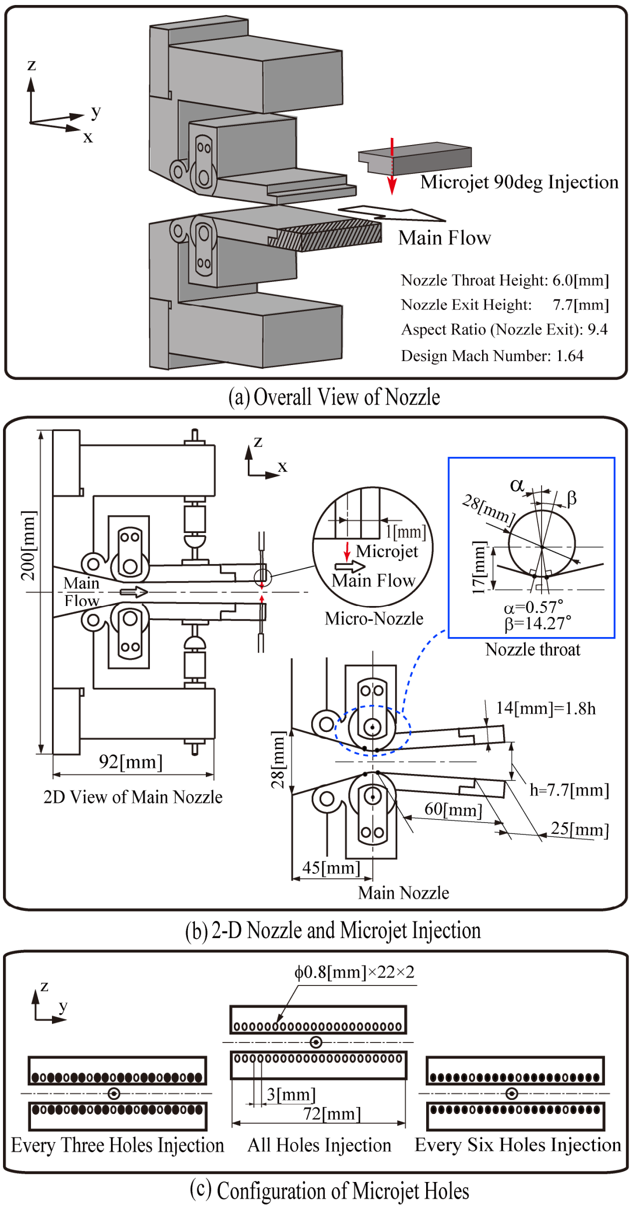

Figure 2 Nozzle with Microjet Injection Holes

investigate effects of non-axisymmetric nozzle shapes. In the case without microjet injection, nearly two-dimensional phenomena are expected so that the microjet effects on the flow fields might be clearly grasped with the simplified configuration. The microjets divided at the manifolds are introduced through convergent micro-nozzles that had diameters of 0.8mm at the nozzle exit. The number of the micro-nozzles is 44 evenly spaced at both the upper and the lower nozzle exits.

The configurations of the microjet injection devices are shown in Fig.2b). In the previous paper, the microjet was injected to the main jet at angles of 60 and 90 degrees[9]. The 90 degrees injection, in which the microjet was perpendicularly injected to the main jet, accomplished notable noise reduction with small amount of microjet[9,10]. As is indicated in Fig.2b), the microjet holes for 90 degrees injection are located on the upper and lower walls of the nozzle. Since it was found that microjet injection from 12 mm and 23 mm upstream of nozzle exit could hardly change the acoustic field, 90 degrees injection from the holes located on 1mm upstream of nozzle exit is focused on in the present study.

The number of the microjet holes was also changed, as shown in Fig.2c), from ‘all-hole’ injection down to ‘every-six-hole’ injection. The corresponding number of microjets was 44 in all-hole injection, 14 in every-three-hole injection, and so on. The smallest number was 6 in every-six-hole injection.

3.2 DATA ACQUISITION AND ANALYSIS

In acoustic measurement, the spectrum and sound pressure of jet noise were measured in the far field with two Bruel & Kjaer (B&K) model 4939 1/4-inch free-field condenser microphones. As shown in Fig.3, they were positioned on the 1/6 spherical surface of a radius of 0.75m. The centre of the sphere was placed on the nozzle exit. The angle θ represents the elevation angle, while the angle ϕ represents the azimuthal angle. The measurement ranges of angles ϕ and θ were from 0 to 120 degrees and 0 to 90 degrees, respectively, with an interval of 10 degrees. However, the measurements were not conducted when microphones were located in the main flow, that is, when both ϕ and θ were smaller than 30 degrees. The frequency range of the acoustic measurement was up to 50 kHz. The detailed setting of acoustic measurement can be found in Ref.10. The acoustic effects of microjets were evaluated by the analysis results of narrow band spectra, SPL (Sound Pressure Level), OASPL (Overall Sound Pressure Level), and sound power level.

Static pressures at the nozzle exit and upstream settling chamber were measured so as to monitor the main jet condition. Mach number was determined from these pressure data on the assumption of isentropic expansion.

The flow field was visualized with shadowgraph technique in order to understand the relation between the noise reduction and the flow field behaviour.

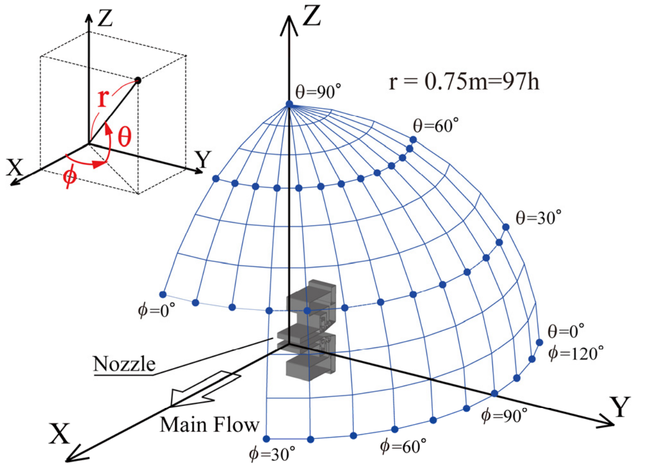

Figure 3 Coordinate system and measurement points

Table 1 Experimental conditions

<table>
<tr><th>P [MPa]
(P_e/P_a)</th><th>P_m[MPa]</th><th>Layout (s/d)
[Number of holes]</th><th>ψ[%]</th><th>Main jet condition</th></tr>
<tr><td rowspan="7">0.41
(1.08)</td><td>-</td><td>-</td><td>0.0</td><td rowspan="7">Under-expanded</td></tr>
<tr><td>0.20</td><td rowspan="2">all holes (3.75)
[44]</td><td>2.9</td></tr>
<tr><td>0.51</td><td>0.67</td></tr>
<tr><td>0.20</td><td rowspan="2">every three holes (11.25)
[14]</td><td>1.0</td></tr>
<tr><td>0.51</td><td>0.26</td></tr>
<tr><td>0.20</td><td rowspan="2">every six holes (22.5)
[6]</td><td>0.47</td></tr>
<tr><td>0.51</td><td>0.11</td></tr>
</table>

3.3 FLOW CONDITION

The total pressure of the main jet and that of the microjet were changed to control the nozzle exit Mach number of the main jet and the mass flux ratio of the microjet against the main jet. The Mach number of the main jet was changed from 1.07 to 1.49. The results in the case of M=1.49 (P=0.41MPa) are discussed below because significant effect of noise reduction was observed when the main jet was under-expanded. The operating conditions are shown in Table 1. Total temperature of main jet and microjet is ambient temperature (approximately 288K). Reynolds number based on nozzle exit height is $4.5*10^5$.

The experiments were conducted for the following three cases; all microjets injected, every three holes of microjets injected, and every six holes of microjets injected as mentioned in 3.1. In Table 1, the parameter s/d means the spacing between two active microjet holes normalized by the diameter of microjet injection holes.

The mass flux of the main jet was estimated by using the throat section area and the settling chamber pressure measured in the experiment, while that of microjet was measured with the mass flow meter.

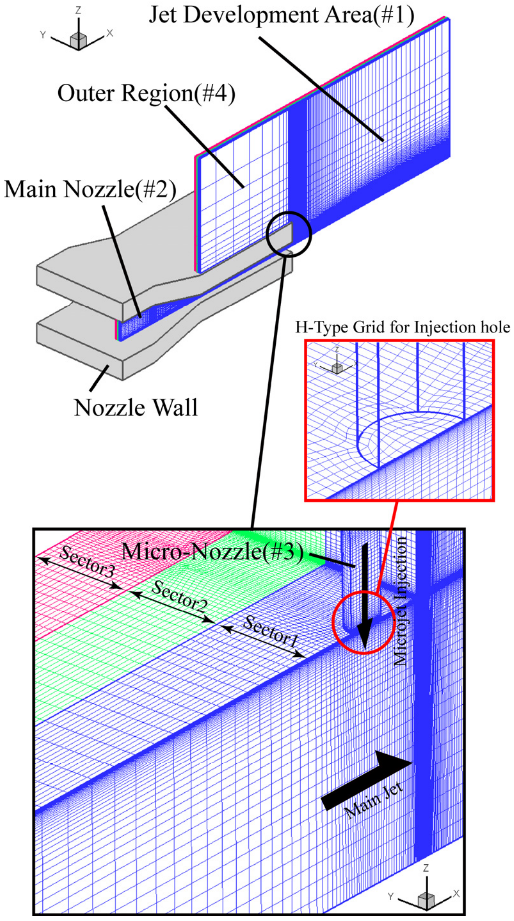

Figure 4 Computational grid

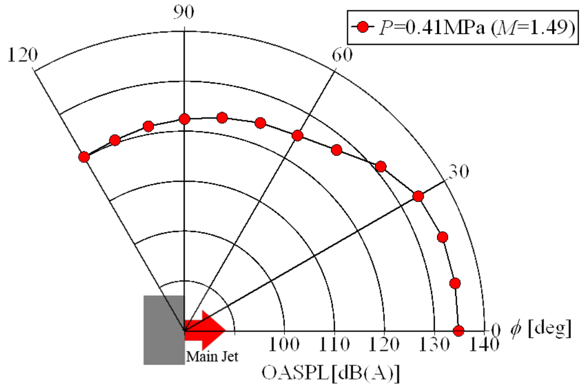

Figure 5 OASPL distribution on θ=30deg plane (w/o microjet)

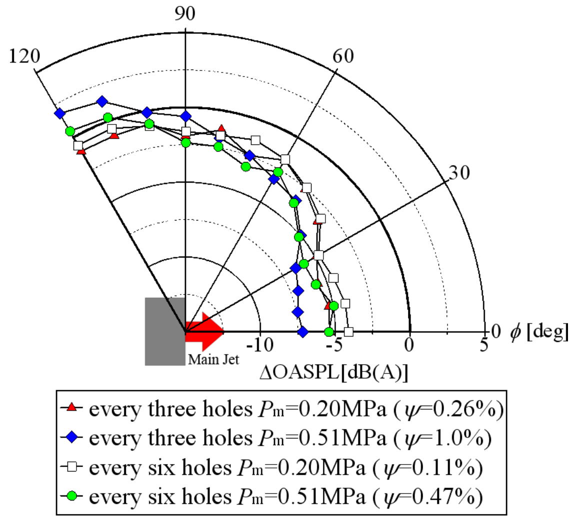

Figure 6 ΔOASPL distribution on θ=30deg plane (M=1.49)

3.4 NUMERICAL METHOD

Steady three-dimensional flow simulations were performed based on compressible Navier-Stokes equations. Details of numerical scheme used in the present study can be found in Ref.10. The grid system is shown in Fig.4. In the figure, three colored 'sectors' used for every-three-hole injection are shown. In the numerical analysis, only the upper half of the main flow was analyzed so as to reduce computation time. The computational region was divided into 'sectors' including a half of the microjet injection hole. Each 'sector' is divided into 4 sub-blocks and the grid size of each block is as follows, jet development area (#1,180*18*120), main nozzle (#2, 240*18*50), micro-nozzle (#3, 6*6*130) and outer region (#4, 20*18*10). The condition of y+=1 is maintained along the nozzle wall. Total number of grid points in the case of every-three-hole injection is about 1840000. In the case of every-six-hole injection, six sectors are used and total number of grid points is 3680000.

At the inlet boundary of the main nozzle, total pressure was fixed to the settling chamber pressure measured in the experiment, and the measured manifold pressure was used as the inlet boundary condition for microjet. In order to match the mass flux of CFD with that of experiment, diameter of micro-nozzle exit was changed. This means that the decrease of the effective sectional area due to the boundary layer was takes into account. The diameter was set to 0.58mm in the case of P_m=0.51MPa and 0.50mm in the case of P_m=0.20MPa.

4. RESULTS AND DISCUSSION

4.1 EFFECTS OF MICROJET ON ACOUSTIC FIELD

Figure 5 shows OASPL distribution in the ϕ direction on θ =30deg plane. It is found that the OASPL is seen to increase monotonously with decreasing ϕ. At the measurement point ϕ=0deg θ=30deg, located right above the main jet, OASPL

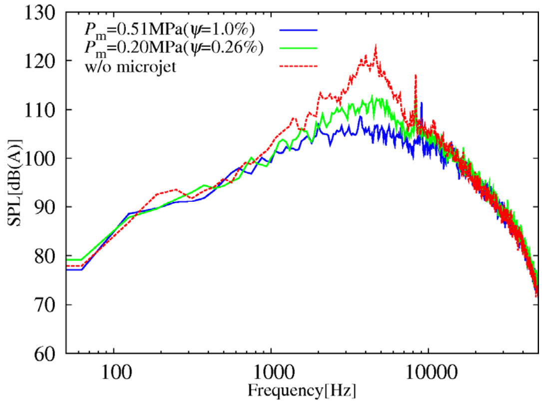

Figure 7 Power spectra at θ=30deg, ϕ=0deg (every three holes injection)

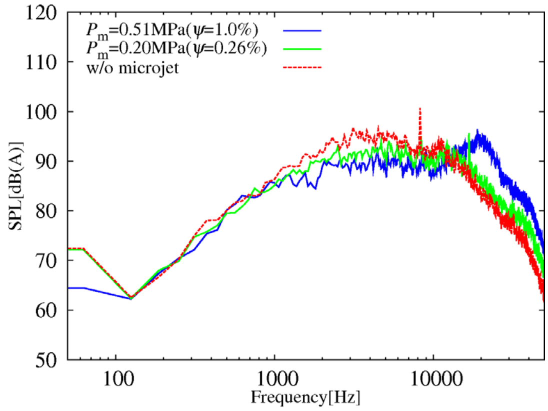

Figure 8 Power spectra at θ=30deg, ϕ=120deg (every three holes injection)

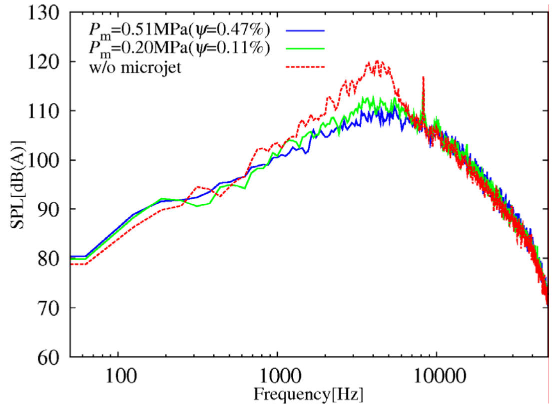

Figure 9 Power spectra at θ=30deg, ϕ=0deg (every six holes injection)

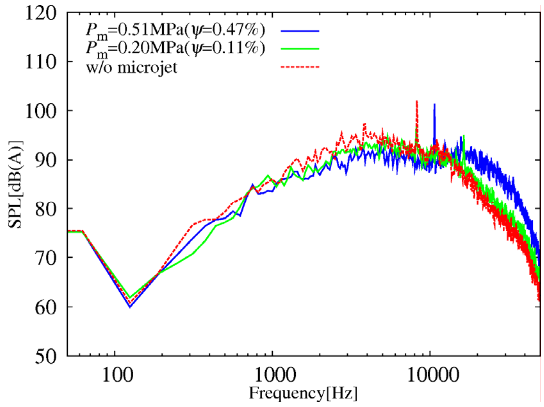

Figure 10 Power spectra at θ=30deg, ϕ=120deg (every six holes injection)

becomes larger than any other measurement point. This tendency of the directivity is consistent with the results of many previous researches[11].

Figure 6 shows ΔOASPL distribution in the ϕ direction on θ =30deg plane. ΔOASPL is defined as the subtraction in OASPL between the cases with and without microjet injection. The negative value of ΔOASPL means noise reduction. The microjets are injected from every three and six holes. As seen in Fig.6, the decrease in the jet noise increases with decreasing ϕ and the maximum reduction is as much as 7.5dB when the microjet was injected from every three holes at the pressure of 0.51MPa. In this case, the mass flux ratio of microjets is 1% against the main jet. In the backward direction of ϕ>100deg, however, the sound pressure is slightly increased by microjet injection. In the case of P_m=0.20MPa and every six holes injection, on the other hand, it can be also seen that maximum reduction is as much as 5dB and the jet noise is hardly increased in the backward direction. In this case, the mass flux ratio is less than 0.5%.

Figure 7 presents the power spectra of the sound pressure in the case of every three holes injection. In the figure, spectra of the cases P_m=0.51MPa, P_m=0.20MPa and the case without microjet are compared. The microphone is located at ϕ=0deg and θ=30deg which is right above the main jet and approximately 7.5dB noise reduction is observed in Fig.6. Figure 8 presents the spectra measured at the position with no OASPL reduction in Fig.6, that is, ϕ=120deg and θ =30deg. In these figures, microjets are injected from every three holes.

In the cases without microjet shown in Figs.7 and 8, the approximate tendency of spectra corresponds to those in the case of fully-expanded main jet, judging from the detailed acoustic measurement of rectangular supersonic jet conducted by Ponton et al.[12]. From the spectrum of the case without microjet in Fig.8, the broadband shock-associated noise, which generally has directivity in the sideline or backward direction of the main jet, is observed to be not remarkable.

Comparing the spectra in Fig.7, the peak noise at the frequency of about 4kHz is considerably reduced in the case of P_m=0.51MPa. Moreover, the screech tone noise is reduced and the frequency of the screech tone noise around 8kHz shifted to a higher frequency. This implies that the shock cell spacing is shortened by microjet. In the case of P_m=0.20MPa, the reduction of broadband peak noise is less than the case of P_m=0.51MPa and the shift of the frequency of the screech tone noise is not measured. These tendencies were seen in the spectra at the measurement point of ϕ=30deg, θ=0deg, that is, in the minor axis direction.

As shown in Fig.8, microjet injection is seen to increase the high frequency noise in the backward direction, though the SPL is reduced as much as 5dB at the frequency of 4 kHz. Power spectra at the points θ=90deg and ϕ=90deg, θ=0deg, that is, in the sideline microphone locations showed similar effects to these of Fig.8. Note that the increase of high frequency noise will be critical in the case of scaling to actual-scale engine.

Figure 9 shows spectra in the case of every six holes injection. The measurement point is the same as Fig.7. While the tendency of peak noise reduction is similar to the case of every three holes injection, the noise reduction in the case of P_m=0.51MPa is less than that of every three holes injection. In the backward direction of the main jet (Fig.10), increase in the high frequency noise is observed, though it is not so prominent as the case of every three holes injection.

4.2 EFFECTS OF MICROJET ON FLOW FIELD

4.2.1 STEADY FLOW FIELD

In the previous studies[9)10)], flow field visualization with schlieren technique was conducted so as to observe the development of mixing layer and the change of shock structure. In the present study, on the other hand, shadowgraph technique was used for the purpose of observing the change of shock structure more clearly. Shadowgraph pictures of two cross sections were taken, that is, x-y plane and x-z plane, as indicated in Fig.11. Figures 12, 13 and 15 show the change in the jet flow field due to microjet injection. Figure 12 presents the flow field of the case without microjet injection. In the top picture of Fig.12, the flow field of the x-y cross section, that is, the long side of the nozzle is shown. Note that the picture shows only half the length of the longer side of the nozzle. In the picture, the shear layer between the main jet and the atmosphere ((A) in Fig.12) and the expansion wave ((B) in Fig.12) generated from the nozzle exit are apparently visible. In the bottom picture showing the x-z cross section, namely, the short side of the nozzle, relatively weak shock cell structure and shear layers are observed.

Figure 13 shows the shadowgraph picture of the case with every-three-hole injection. The total pressure of microjet is set as P_m=0.51MPa. From the bottom picture of Fig.13, it is seen that the shock structure has been obviously changed. Bow shocks ((A) in Fig.13) are observed near the microjet injection holes and Mach shock waves ((B) in Fig.13) are formed by microjet injection. As assumed from the frequency shift of the screech tone noise in Fig.7, the shock spacing is shortened by microjet injection. Furthermore, shock structures are clearly seen to be strengthened at the downstream region of the main jet.

From the top picture of Fig.13, it is also found that the mixing layer is not developed uniformly in the x-y cross section because there are difference in shading of the picture between the downstream flow field of injection holes and the other region. Figure 14 indicates CFD result of Mach number contours at y-z cross-sections of several stations. The upper half of the contour of each streamwise station presents the Mach number distributions in the case that P_m=0.51MPa microjet is injected at an angle of 90 degrees. The lower half presents those in the case without microjet injection. It is shown that the shear layers are changed to wavelike configurations and the flow field becomes non-uniform in the long side direction of the nozzle. It can be seen that microjets

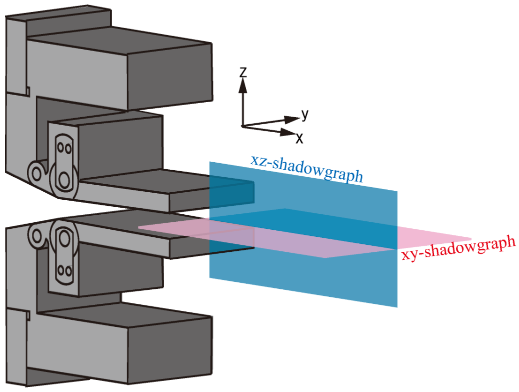

Figure 11 Schematic diagram of planes for shadowgraph photography

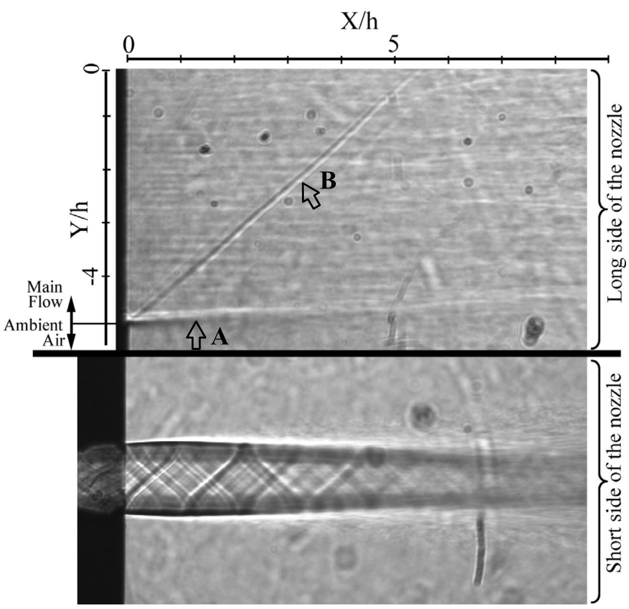

Figure 12 Shadowgraph picture (w/o microjet)

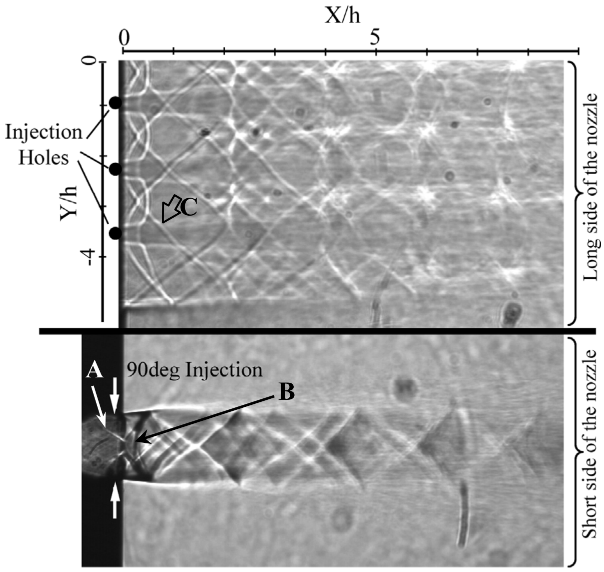

Figure 13 Shadowgraph picture
(90deg every three holes injection, P_m=0.51MPa)

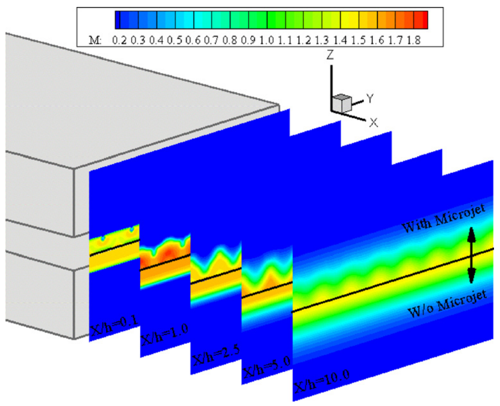

Figure 14 Mach number contours at *yz* cross-section of several stations (CFD)
Upper contour: every three holes P_m=0.51MPa
Lower contour: w/o microjet

penetrate into the main flow, raise the flow and promote the mixture of the main jet and the ambient air.

Shock structure generated by microjet injection influences downstream flow field of adjacent microjet injection holes ((C) in Fig.13). That is to say, the shock structure was changed to be three-dimensional and the uniformity of the flow field was broken by microjet injection.

Figure 15 shows the shadowgraph picture for the case of every-six-hole injection. The total pressure of microjet was set at P_m=0.51MPa. It can be seen from the short side picture that the shock wave is obviously weaker than that of every three holes injection. However, the shock strength of the long side are intense and its structure has three-dimensional

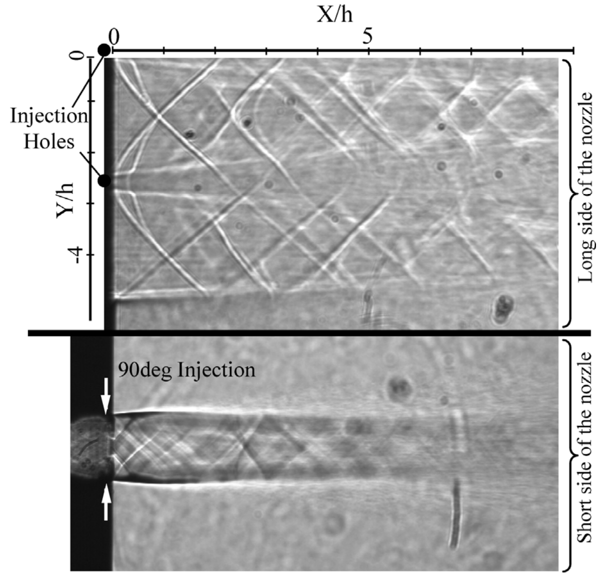

Figure 15 Shadowgraph picture
(90deg every six holes injection, P_m=0.51MPa)

characteristics similar to that of every-three-holes injection case.

4.2.2 THRUST LOSS

Thrust loss due to microjet injection was estimated on the basis of steady CFD analysis. The flow fields of four cases (hatched in Table 1) and their thrust loss were analyzed. Figure 16 shows the configuration of computational region and control volume for thrust estimation. The upper figure corresponds to the case with microjet injection and the lower indicates the case without microjet. The inlet of the control volume was set at the position where flow velocity is equal to zero. First of all, the thrust in the case with microjet was given by the following equation:

$$F_{with} = [I_{e1} + I_{e2} - I_i]_{with} = [\dot{m}_e u_e + (P_e - P_a) A_e]_{with} \quad (1)$$

where $\dot{m}_e$ u_e and A_e mean the mass flux, velocity and sectional area at the nozzle exit, respectively.

On the other hand, in the case without microjet, the thrust in the case that microjet is injected parallel to the main jet axis was added for proper comparison of thrust force in both cases. Consequently, the thrust in the case without microjet was calculated as follows:

$$F_{w/o} = [I_{e1} + I_{e2} - I_i]_{w/o} + I_{e3} \quad (2)$$

Here, I_{e3} means the impulse function at the exit of micro-nozzle in the case that microjet was injected parallel to the main jet axis. CFD analysis for micro-nozzle was carried out and the physical quantity of the micro-nozzle exit was used for the evaluation of I_{e3}. Thrust loss was obtained by following formula:

$$Thrustloss[\%] = \frac{F_{w/o} - F_{with}}{F_{w/o}} \times 100 \quad (3)$$

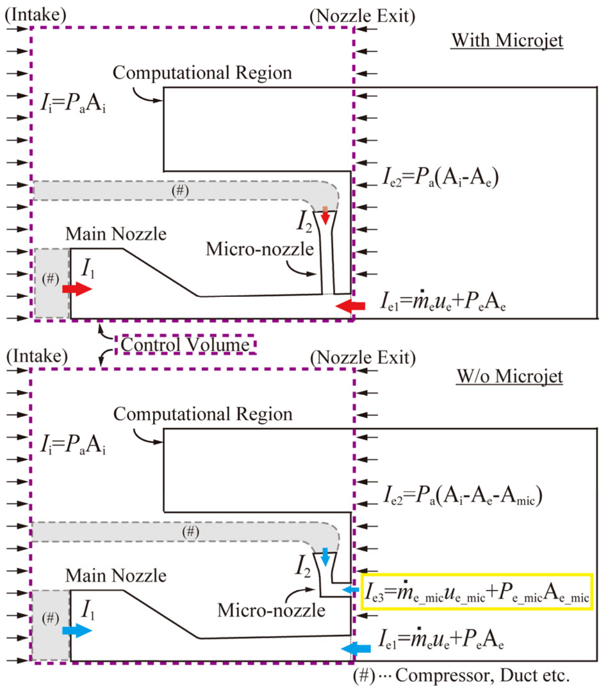

Figure 16 Schematic diagram of control volume used for thrust estimation

The thrust loss in the present model means the loss due to the mixing of the main jet and microjet. Figure 17 shows the relation between mass flux ratio and thrust loss. It can be said from this figure that the thrust loss seems almost proportional to the mass flux ratio. In Fig.18, mass flux ratio and reduction of the sound power level are compared in the cases with every three and six holes injection. The definition of sound power level is mentioned in Ref.10. When microjet total pressure is set at P_m=0.51MPa, every-three-hole injection reduces more total acoustic energy generated into the atmosphere than every-six-hole injection. Considering the application of microjet, however, the mass flux ratio and thrust loss could be a crucial parameter. Hence, the every-six-hole injection might have a promising possibility to achieve the large noise reduction and minimize the influence on the overall engine performance.

4.2.3 UNSTEADY FLOW FIELD

In order to investigate the unsteady behavior of the flow field, shadowgraph pictures were taken by using a high speed camera (FASTCAM-APX RS from Photron Ltd.). Frame rate and shutter speed were set to 36000fps and 1/153000sec, respectively.

Figure 19 shows the shadowgraph pictures of the case without microjet in which consecutive 5 frames are shown. Figures 20 and 21 show the shadowgraph pictures of the case with every-three-hole and every-six-hole injection,

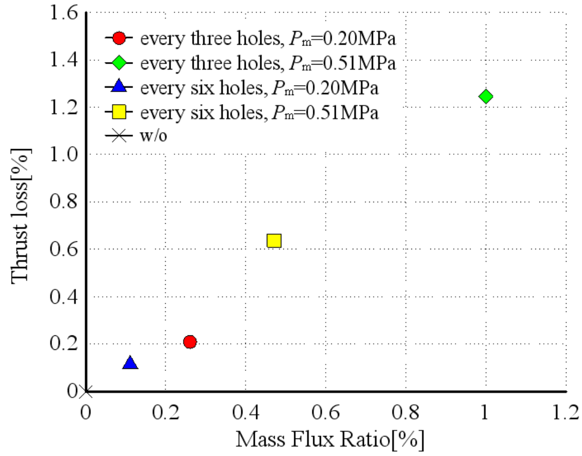

Figure 17 Relation between mass flux ratio and thrust loss

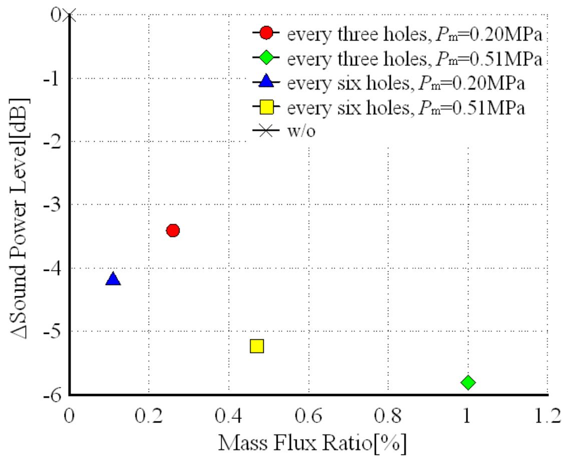

Figure 18 Relation between mass flux ratio and sound power level

respectively. In these cases, microjet pressure was set to 0.51MPa.

Figures 19, 20 and 21 clearly indicate that large fluctuations of jet shear layers in the case without microjet were suppressed by microjet injection. Since noise source of screech tone is said to be the large fluctuation of the jet flow, it is supposed that such suppression effect of microjet alleviates screech tone noise in the far acoustic field. Furthermore, large-scale coherent turbulence structures can be seen in Fig. 19. On the other hand, these structures are not visible in the case with microjet. Figure 14 shows that the configuration of shear layers is changed by the addition of momentum at the constant spacing in the long side of the nozzle. It is predicted that this

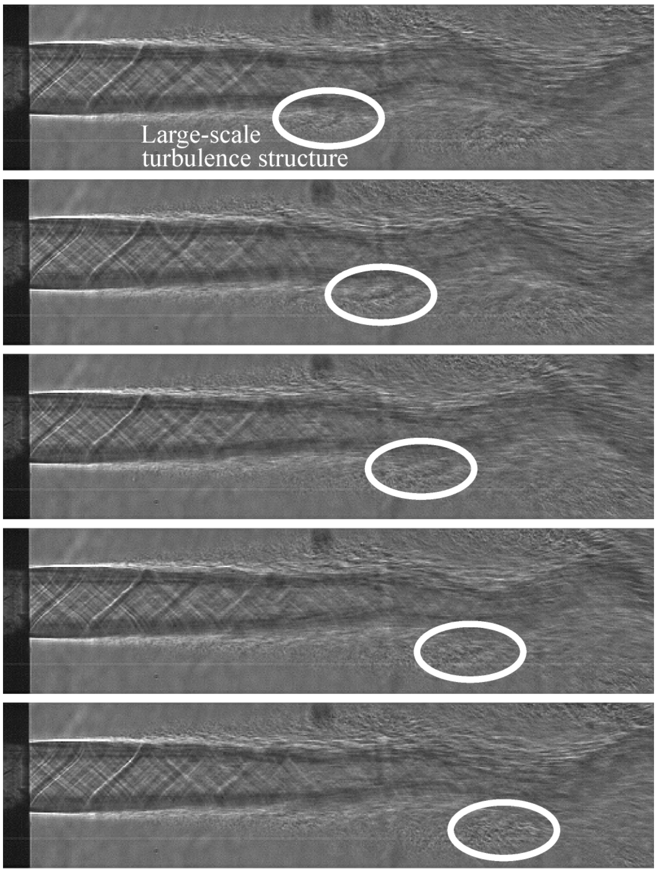

Figure 19 Instantaneous shadowgraph pictures in the case without microjet
(δt=1/36000sec)

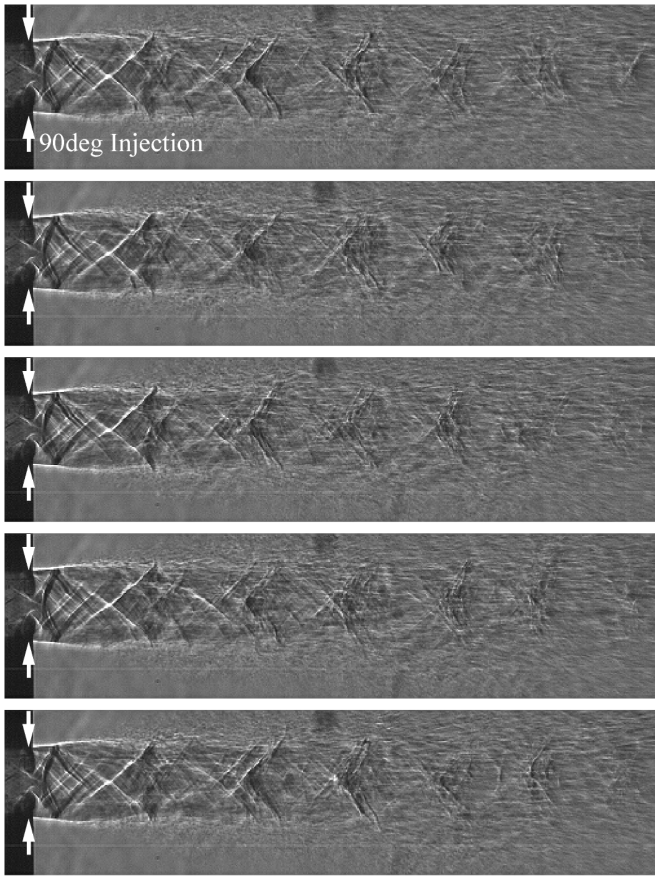

Figure 20 Instantaneous shadowgraph pictures in the case with microjet (every three holes, P_m=0.51MPa)
(δt=1/36000sec)

effects suppress the development of large-scale turbulence structures in the shear layer. Since Tam et.al.[11] pointed out that large-scale turbulence structures are the noise source of the peak noise in the downstream direction of the main jet, it is thought that the large noise reduction at the frequency of 4 kHz is caused mainly by the suppression of the large-scale turbulence structures.

However, the reasons why the increase in high-frequency noise was not detected at the measurement point of the downstream, and why the flow field of Figs.13 and 15, in which cases shock waves were strengthened, did not generate the intense shock-associated noise were not understood yet. For further study to understand the mechanism of microjet effect, detailed measurement and unsteady RANS or LES analysis will be performed in the future work.

5. CONCLUSIONS

The effect of microjet injection on jet noise was experimentally studied for a rectangular supersonic jet for a jet Mach number of 1.49. The injection angle of the microjet to the main jet was set to 90 degrees. In order to investigate the mechanism of noise reduction by microjet injection, flow field visualization with shadowgraph technique and steady CFD analysis of the flow field were conducted. The conclusions are summarized as follows.

1. Jet noise was reduced by the use of microjet injection. The reduction of the overall sound pressure level was up to approximately 7.5dB. In this case, the mass flux ratio of the microjet and the thrust loss were 1% and 1.25%, respectively. Noise reduction of 5dB was observed even in the case with mass flux ratio of 0.47%. The thrust loss was 0.64% in this case.

2. The noise component around the frequency of 4 kHz was greatly reduced. The high frequency turbulent mixing noise was, however, increased significantly due to microjet injection in the backward direction of the main jet.

3. From the results of steady shadowgraph visualization, it was found that shock wave was strengthened, and that the mixing layer became non-uniform in the long side direction of the nozzle.

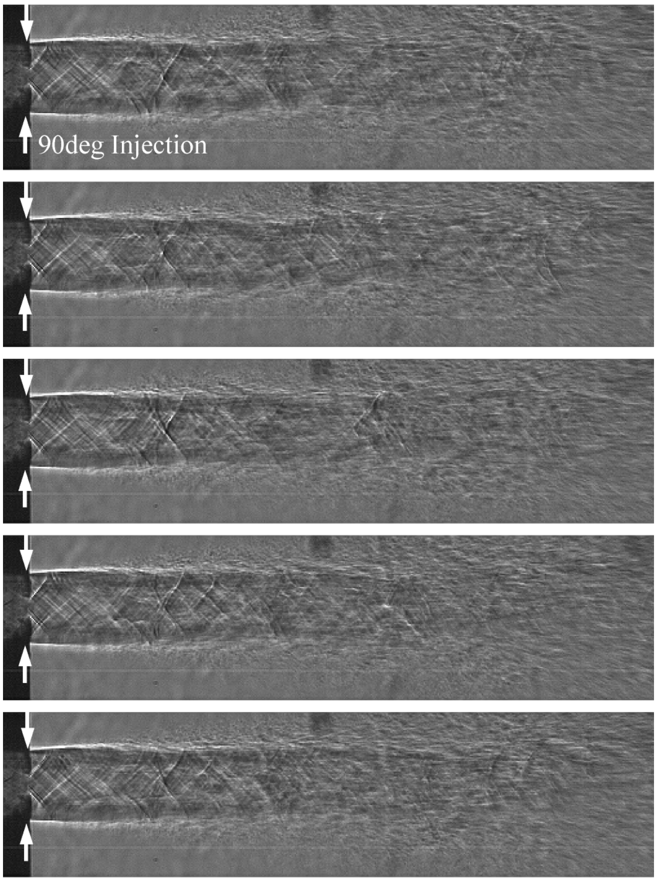

Figure 21 Instantaneous shadowgraph pictures in the case with microjet (every six holes, P_m=0.51MPa) (δt=1/36000sec)

4. The unsteady flow field visualization showed that microjet suppressed large fluctuation of jet shear layers and the development of large-scale turbulence structures.

ACKNOWLEDGMENTS

The present work was partially supported by Grant-in-Aid for Scientific Research (B) (No.20360381). The authors wish to thank Japan Society for the Promotion of Science for the financial support.

REFERENCES

1) Massey, K. C., Ahuja, K. K. and Messersmith, N.,: Forward Flight Effects on Heated and Unheated Rectangular Nozzle, AIAA Paper 2002-2517 (2002).

2) Ahuja, K. K. and Brown, W. H.,:Sear Flow Control by Mechanical Tab, AIAA Paper 89-0994 (1989).

3) Loheac, P., Julliard, J. and Dravet, A.,: CFM56 Jet Noise Reduction with the Chevron Nozzle, AIAA Paper 2004-3044 (2004).

4) Alvi, F. S., Elavarasan, R., Shih, C., Garg, G. and Krothapalli, A.: Active Control of Supersonic Impinging jets Using Microjets, AIAA Paper 2000-2236 (2000).

5) Castelain, T., Sunyach, M., Juve, D. and Bera, J.: Effect of Microjets on a High-Subsonic Jet. Parametric Study of Far-Field Noise Reduction., AIAA Paper 2006-2705 (2006).

6) Greska, B. and Krothapalli, A.: The Effects of Microjet Injection on an F404 Jet Engine, AIAA Paper 2005-3047 (2005).

7) Zaman, K. B. M. Q.,: Jet Noise Reduction by Microjets – A Parametric Study, AIAA paper 2009-3129 (2009).

8) Zaman, K. B. M. Q. and Podboy, G. G.,: Effect of Microjet Injection on Supersonic Jet Noise, AIAA paper 2010-4022 (2010).

9) Watanabe T., Okada R., Uzawa S., Himeno T. and Oishi T.: Experimental Study of Supersonic Jet Noise Reduction With Microjet Injection, ASME GT 2009-59436 (2009).

10) Okada R., Watanabe T., Uzawa S., Himeno T. and Oishi T.: Investigation of Microjet Injection for Reduction of Supersonic Jet Noise, ASME GT 2010-23036 (2010).

11) Tam, C. K. W.: Supersonic Jet Noise, Journal of Fluid Mechanics, vol.27, (1995), pp17-43.

12) Ponton, M.K. Manning, J.C. and Seiner, J.M.: Far-Field Acoustics of Supersonic Rectangular Nozzles With Various Throat Aspect Ratios, NASA Technical Memorandum 89002.